JOURNAL OF THERMOPHYSICS AND HEAT TRANSFER
Vol. 15, No. 4, October–December 2001

Emission and Raman Spectroscopy Measurements in Hypersonic Nitrogen Flows

H. Pilverdier,* R. Brun,† and M. P. Dumitrescu‡
Université de Provence, 13453 Marseille, France

The self-luminosity of nitrogen hypersonic flows in the free-piston shock tunnel TCM2 at Marseille is analyzed for different enthalpy conditions. To perform vibrational population measurements in these flows by spontaneous Raman spectroscopy (SRS), the intensity of this emission is tentatively reduced by acting on various technical parameters and flow conditions. Thus a few low-enthalpy conditions are defined for which the SRS method can be used without being disturbed too much by the flow emission at the nozzle exit and behind the bow shock of a blunt body. For these conditions the vibrational populations of the first several vibrational levels of nitrogen are determined during the steady phase of the flow: The vibrational temperatures defined from the population of these levels correspond to the values given by classical computations assuming Landau–Teller models, that is, the expected frozen value at the nozzle exit and a value close to equilibrium behind a bow shock. However, an overpopulation of the highest levels cannot also be excluded.

Nomenclature

A	=	nozzle area
A^*	=	critical nozzle area
M_s	=	shock Mach number
N_p	=	number of detected photons
N_v	=	vibrational population of the v level
P_0	=	stagnation pressure behind the reflected shock
T	=	translational temperature
T_r	=	rotational temperature
T_v	=	vibrational temperature
T_0	=	stagnation temperature behind the reflected shock
t	=	time with origin taken at the shock reflection at the end of the shock tube
σ	=	standard deviation

Introduction

BEFORE using spectroscopy diagnostic methods in high-enthalpy hypersonic facilities, it is necessary to perform spectrally resolved studies of the flow luminosity generally present in these facilities.[1,2] Thus, the first aim of this study was to analyze this self-luminosity for the enthalpy conditions previously used in the free-piston shock tunnel TCM2 at Marseille (3.5 and 11 MJ/kg corresponding to conditions 1 and 2 in Table 1).[3,4] This facility uses a free piston to obtain a high-pressure and a high-temperature driver gas.[5] The ultimate purpose was to perform vibrational population measurements (N_2, O_2, NO) in the airflow at the exit of the nozzle in the Mach number range 6–8 and also along the stagnation line of a hemispherical body by a spontaneous Raman spectroscopy (SRS) method. It was therefore necessary to know if the observed radiation could conceal the Raman lines. Thus, the emission of a nitrogen flow corresponding to already defined enthalpies (running conditions 1 and 2, Table 1) is first recorded during the steady phase of this flow in the spectral range centered on 500 nm covering the Stokes and anti-Stokes lines. Then, taking into account the emission intensity, various means are used to reduce this emission to a minimum. Various changes on the technical parameters are made, like improving the cleaning process of the facility and acting on the nature and the mounting of the diaphragm separating the shock tube from the nozzle. However, it is impossible to avoid the presence of the secondary diaphragm separating the shock tube from the nozzle and also to change the nature of the compression and therein the heating of shock-tube walls, which are the source of significant pollution of the test gas. Other means acting on the flow conditions are also tested: The simplest one is to decrease the stagnation enthalpy, because increasing the reservoir pressure and thereby increasing the Raman line intensity relatively to the flow emission is not sufficient because then line overlapping is observed. Thus, new lower stagnation enthalpy conditions are tested corresponding to lower pressure and temperature inside the shock tube in order to decrease the spontaneous emission without significantly decreasing the vibrational excitation and the possible nonequilibrium. Finally, only the flow at the nozzle exit corresponding to conditions 1 in Table 1 is accessible to a Raman analysis to the exclusion of the bow-shock region; New running conditions (conditions 3, Table 1) are also defined corresponding to an incident shock Mach number of 1.7, for which Raman measurements are possible behind a bow shock.

Thus, the second aim of this study is the determination of relative vibrational populations in a nitrogen flow from SRS method in the already defined cases, either at the nozzle exit (conditions 1) or along the stagnation line of a blunt body (conditions 3). The experimental analysis of hypersonic expanding flows in vibrational nonequilibrium has been the subject of many investigations for more than 30 years[6] and, still now, gives rise to controversial conclusions as for the relaxation process in compression and in expanding conditions: all experimental results concerning the vibrational relaxation times, assumed to describe the process by the Landau–Teller formulation, have been obtained in a shock-tube environment, that is, in compression conditions.[7] These values of relaxation times, when applied to situations of expanding flows in nozzles, did not agree with the experimental results, which present also discrepancies with results coming from simulations taking into account a level-by-level relaxation.[8] This was the case, for example, for the oldest experiments,[6,9] which led the respective authors to the conclusion that the relaxation times in nozzles were much shorter than expected from shock-tube experiments and that, therefore, the expanding flows were closer to equilibrium. In fact, these results were deduced from indirect measurements by different techniques, like sodium line reversal,[6] electron beam,[10] or tracer emission.[9,11] Recently, a direct method of measurement of vibrational populations by an SRS method was used, and the conclusion was that there was no difference between global relaxation times

Received 15 May 2000; revision received 8 May 2001; accepted for publication 8 May 2001.

*Ph.D. Graduate, Institut Universitaire des Systèmes Thermiques Industriels, 6595 CNRS, Cedex 13.

†Professor Emeritus, Institut Universitaire des Systèmes Thermiques Industriels, 6595 CNRS, Cedex 13.

‡Research Engineer, Institut Universitaire des Systèmes Thermiques Industriels, 6595 CNRS, Cedex 13. Senior Member AIAA.

in compression or expansion situations, even if the anharmonicity effects and nonresonant vibration-vibration exchanges were taken into account.[12] However, most "old" experiments were performed in "strong" expansion conditions corresponding to usual reflected shock tunnels, and the last one was made in a so-called clean shock tube fitted with a nozzle of low area ratio ($A/A^* = 12$). Together with different impurity level in facilities, this might explain the observed discrepancies about the frozen value of the vibrational temperature.

Experimental Facility and Diagnostic Techniques

The experiments are performed at the exit of the nozzle of the TCM2 facility at Marseille, France (Fig. 1), which has been previously described[4] as has been its associated equipment.[3]

Several test condition sets are defined to obtain steady-state conditions behind the reflected shock at the end of the shock tube as long as possible. The high-pressure, high-temperature gas is used as a reservoir gas to be expanded in a nozzle in order to generate a hypersonic flow. A 693-mm-length conical nozzle with an area ratio of 164 is fitted at the end of a 70-mm-diam shock tube, giving a freestream Mach number of 6 for the conditions 2 (Table 1). The emission measurements are performed with the experimental setup sketched in Fig. 2. Except the exciting laser, this setup is identical with the one used further for the SRS measurement, and the apparatus as a whole is described hereafter (Fig. 2).

The collection system includes a spatial filter to select the scattering volume of interest, a holographic sharp-edge notch filter with an optical density of 6 at 500.0 nm, more than 75% transmission outside the notch, and a second lens to adapt the collected beam to the acceptance cone of a Jobin-Yvon HR 640 monochromator. At the exit of the HR 640, a double-intensified diode array, Princeton Instruments D/SIDA 1000, cooled at -25°C, receives the 25-mm-wide spectral window on its 1024 diodes. The gratings used are blazed at 500 nm. One system has a grating carved at 600 lines/mm, and the other has a grating carved at 1200 lines/mm.

For SRS measurements a single-pulse flash lamp pumped Candela dye laser is used as incident radiation source to obtain as many as possible incident photons keeping incident power well below air breakdown (10 W/m^2). The laser gives up to 16 J in 6 μs at 500 nm, with a spectral line width of 0.07 nm. The laser beam, vertically polarized, parallel, and located above the shock-tunnel axis, is vertically reflected toward the experiment chamber. It is focused in the hypersonic freestream at the nozzle exit or 4 mm in front of the model on the stagnation line. The irradiated volume is 1.5 mm height and 0.6 mm diam. It is imaged on both sides of the facility (Fig. 2) through identical collection systems giving a 90-deg observation angle configuration. To increase the signal/noise ratio, the intensifiers of the detectors are gated simultaneously during 7 μs inside the laser pulse duration, thus capturing 70% of the total incident energy. Before each run, the laser energy and the whole optical system are checked.

Table 1 Conditions of SRS experiments

Conditions	M_s	P_0, Mpa	T_0, K
1	5.0	17	2900
2	9.0	50	6500
3	1.7	7	600

Luminosity Experiments and Reducing Parameters

Emission spectra with the conditions 2 present a very high background level with important individual lines essentially coming from metallic impurities, calcium, sodium and silicon so that these conditions have no longer been used. Similar levels of self-luminosity have been encountered in other comparable facilities.[1,2]

An example of spectrum obtained in the range 535–595 nm for the conditions 1 at the nozzle exit is represented in Fig. 3 and also presents an important emission. However, it has been possible to reduce this emission, partly coming from the mylar secondary diaphragm separating the shock tube from the nozzle, which completely disappears after the shock reflection and gives rise to strongly radiating organic molecules or radicals, even, apparently, during the steady phase of the flow.

Different materials constituting the secondary diaphragm were tested, and it was found that the metallic sheets give the best results. An aluminum diaphragm is quickly partially liquefied, breaks into many melted scraps dangerous for models, and is also the origin of an important radiation. Finally, a 100-μm-thick copper diaphragm was

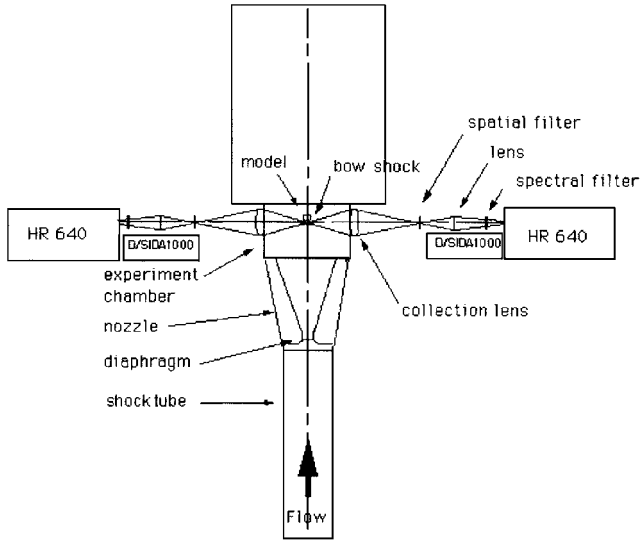

Fig. 2 Experiment chamber and collection systems.

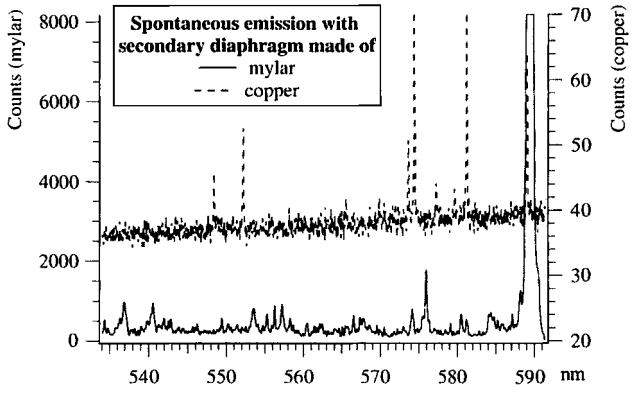

Fig. 3 Spontaneous emission at 4 mm in front of the model using organic or copper for the secondary diaphragm.

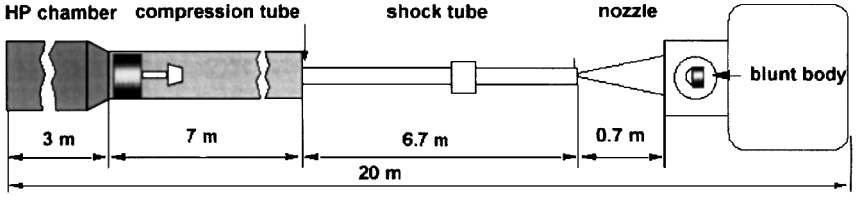

Fig. 1 Scheme of TCM2 facility.

chosen, owing to its higher thermal capacity and its higher melting point and resulting low emission as seen in Fig. 3. In both cases the running conditions of the facility are conditions 1, which correspond to a stagnation temperature of 2900 K, but the integration time of the run with the copper diaphragm is 100 μs (from $t = 750$ to 850 μs), whereas it is 7 μs (from $t = 800$ to 807 μs) in the run with mylar diaphragm. Moreover, a circular score with a nonuniform depth enables the diaphragm to be ejected outside the nozzle axis. Another important parameter contributing to a reduction of luminosity is obviously a careful and systematic cleaning of the facility after each experiment.

Of course, the influence of the stagnation temperature on the radiation level is also very important and weakly depends on the nature of the test gas, argon or nitrogen. In this way two examples of the spontaneous emission in the same spectral range obtained with the same collection setup parameters, that is, essentially the same integration time, monochromator slit height, and width, are given in Fig. 4 coming respectively from nitrogen flow and argon flow in front of the hemispherical model. The respective stagnation temperatures are 7000 K (argon) and 2900 K (nitrogen): identical lines appear in both spectra, but they are considerably amplified in the case of argon flow for which the temperature is higher.

It is very difficult to identify atoms and molecules responsible of all parasitic lines because the possible pollutants are numerous. However, among the most intense lines the 541-nm line can be ascribed to chromium, the 559 nm to aluminium, the 578 nm to copper, the 589 nm to sodium. This obviously comes from the various materials composing the tunnel and its accessories, as well as from environment (calcium, sodium). Another independent parameter, which is responsible for increase of radiation, is the laser itself used for Raman experiments: it may excite not only nitrogen molecules but also various impurities, thus noticeably increasing the radiation level of the corresponding molecules. An example is represented in Fig. 5. Because of this effect, Raman experiments cannot be correctly interpreted behind a bow shock with conditions 1.

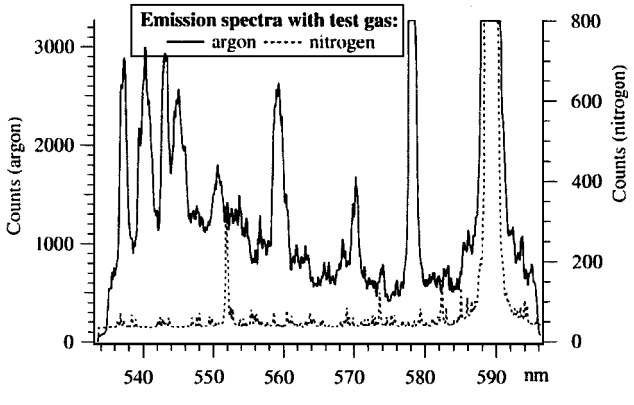

Fig. 4 Spontaneous emission at 4 mm in front of the model using nitrogen or argon as test gas.

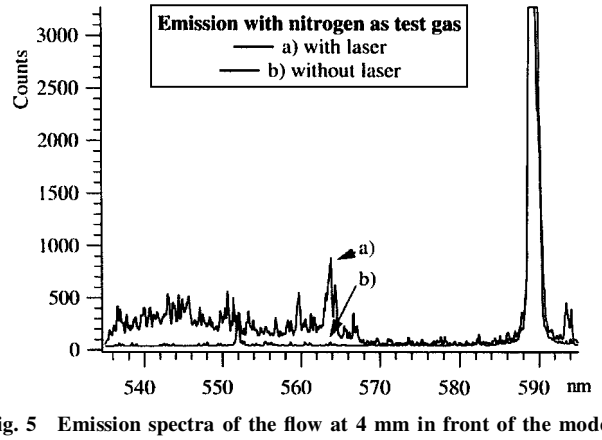

Fig. 5 Emission spectra of the flow at 4 mm in front of the model: conditions 1, with and without laser.

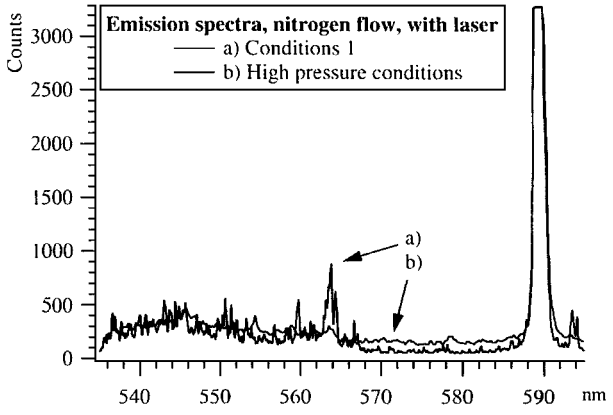

Fig. 6 Emission spectra of the flow at 4 mm in front of the model with laser: conditions 1 and high-pressure conditions.

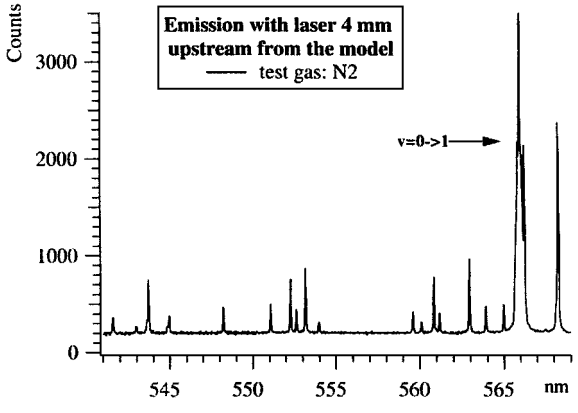

Fig. 7 Emission spectra of the flow at 4 mm in front of the model with laser: conditions 3.

On an attempt to increase the intensity of Raman spectra, the initial pressure in the shock tube is increased in order to increase the reservoir pressure: new conditions were so defined, these conditions giving high reservoir pressure 56 ± 5 Mpa but the same reservoir temperatures as in conditions 1. In Fig. 6 Raman lines obtained with these high-pressure conditions (reservoir pressure three times higher than pressure of conditions 1) depict an increased intensity, but their overlapping with background lines (themselves magnified) prevents any reliable population measurement.

Finally, as just indicated, the low-enthalpy conditions, that is, conditions 3, Table 1, have been chosen for Raman measurements behind a bow shock: they correspond to an incident shock Mach number of 1.7 with reservoir pressure and temperature of respectively 7 Mpa and 600 K, and at the nozzle exit to local translational-rotational temperature and static pressure respectively of about 50 K and 10 Pa. An example of the Stokes Raman spectrum in front of a hemispherical model (5.6-cm radius) is presented in Fig. 7. Like all similar experiments, the laser is started during the steady phase of the flow, and the light is collected during 7 μs. For this case the obtained spectrum includes only a few lines, and the more intense corresponds to the transition $0 \rightarrow 1$ from the Raman Stokes Q branch of nitrogen. Other higher transitions are also visible, but a few emission lines remain. In conclusion, nitrogen flow with conditions 1 at the nozzle exit and with conditions 3 behind a bow shock can be used for Raman tests, which are described hereafter.

Experimental Flow Conditions

The experimental conditions 1 and 3 defined in Table 1 must be assessed by complementary experiments in order to be sure that Raman spectra correspond to a reliable and known environment. Thus, various pressure measurements (stagnation region, nozzle wall, and pitot pressure) are performed and reported here, as well as time-resolved spectra recorded during the shot.

Pressure Measurements

First, it is necessary to be sure of the constancy of the stagnation pressure during a sufficiently long time .This seems to be the case when considering the pressure plateau in Fig. 8 lasting 700 and 1500 μs, respectively, for conditions 1 and 3 and corresponding, more or less, to tailored conditions in the shock tube. It is the same for pitot pressures reported in Fig. 9 exhibiting quasi-constant values during 300 and 1000 μs, respectively. A pressure increase and a fluctuating period precede this steady phase and correspond to the nozzle startup and the flow establishment around the model. However, sole pressure measurements cannot give reliable information on the arrival of the contact surface separating the driver and driven gases and must be correlated with other experimental means (see the following).

Static-pressure measurements are also performed along the nozzle walls for conditions 1, and their values during the steady phase are represented in Fig. 10. In the same figure they are also compared with measurements obtained with air as a test gas for the same reservoir pressure and temperature: The corresponding values remain 10% smaller than in pure nitrogen case, thus confirming that stronger real-gas effects exist in the air case, recombinating oxygen being the cause of a weaker expansion.

These measurements are in good agreement with the results given by a Navier–Stokes numerical computation including Park chemistry[13] and a simple Landau–Teller vibration model with Shatalov vibrational relaxation times.[14] This calculation was performed by William[15] using the experimentally measured reservoir parameters with air and nitrogen as test gases and the results are reported in Fig. 10. This graph shows the deviation between both cases, which is the same as found in experiments, and only a small discrepancy appears between computations and experiments at the beginning of the expansion.

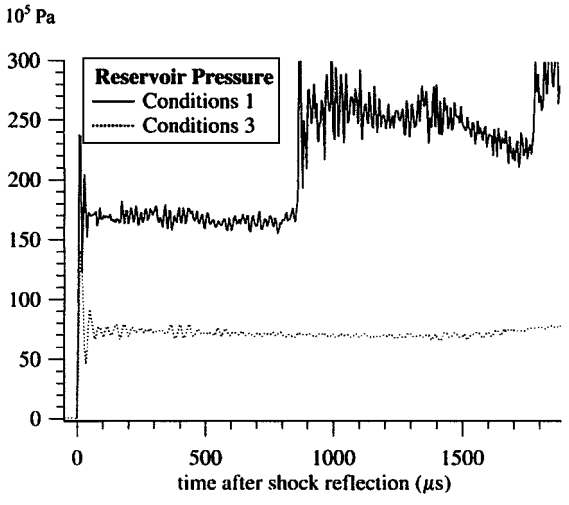

Fig. 8 Time evolution of reservoir pressure in conditions 1 and 3.

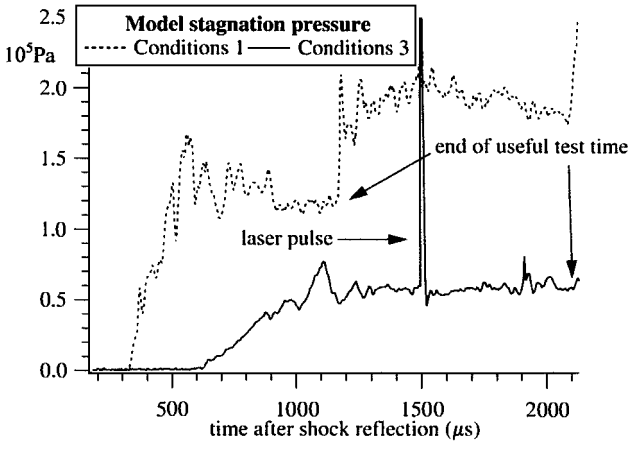

Fig. 9 Time evolution of model stagnation pressure in conditions 1 and 3.

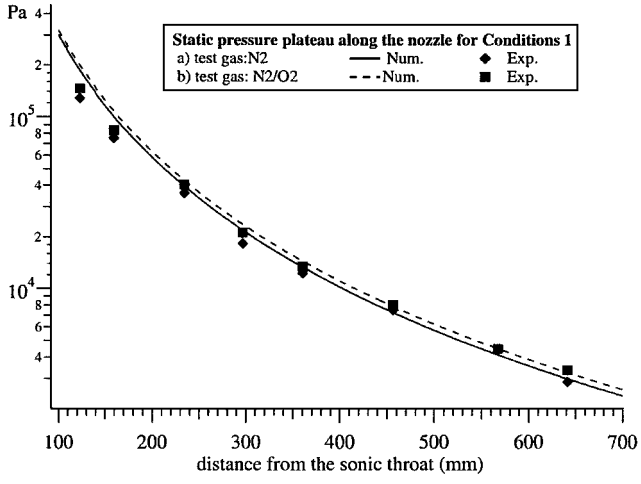

Fig. 10 Evolution of static pressure along the nozzle in conditions 1 using nitrogen or air as test gas.

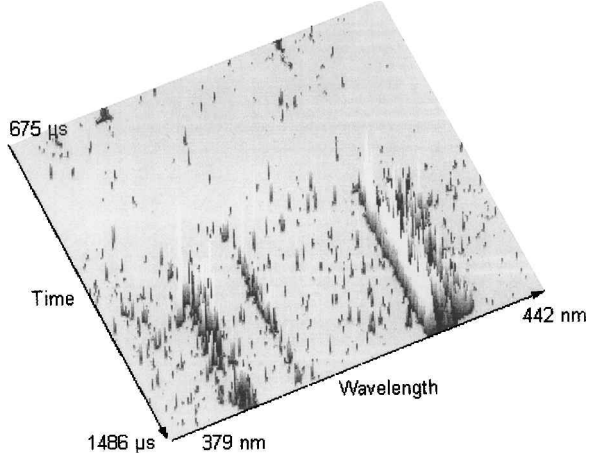

Fig. 11 Time evolution of emission spectrum at 4 mm in front of the model: conditions 1.

Time-Resolved Emission Spectra

Pressure measurements have been followed by a time-resolved recording of a large spectral range of the flow emission, thus the history of the most important lines can be easily analyzed, in particular their appearance and vanishing. The experimental setup is the same as already used (Fig. 2), but a streak camera system placed at the exit of the monochromator gives the time evolution of a spectrum part. For this, the monochromator is centered at 410 nm giving a spectral window from 379 to 442 nm, and the record begins at $t = 675$ μs (i.e., 675 μs after the shock reflection at the end of the shock tube). Three-dimensional images are then obtained. An example corresponding to conditions 1 is represented in Fig. 11. As expected, the emission is weak during the first 400 μs after the starting of the registration, that is, about 1.1 ms after the shock reflection. Then, the observed steep increase of the emission comes from the mixing zone constituting the contact surface known to be strongly luminous particularly after its interaction with the reflected shock.[16] This increase is quasi-synchronous with the pitot-pressure increase (Fig. 12) so that this increase can be considered as the end of the useful steady flow time. The time record performed for the most intense band of the spectrum (424–432 nm), compared with pitot-pressure evolution, confirms these conclusions (Fig. 12). Thus, the steady phase of the nitrogen flow can be clearly delimited. From the Pitot-pressure records (Fig. 9), confirmed by the nozzle-wall

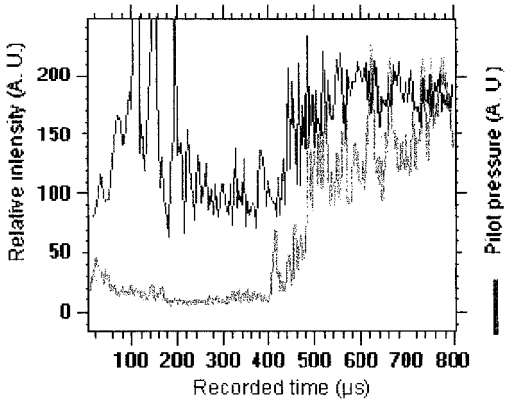

Fig. 12 Time evolution of pitot pressure and of the most intense emission band (424–432 nm): conditions 1.

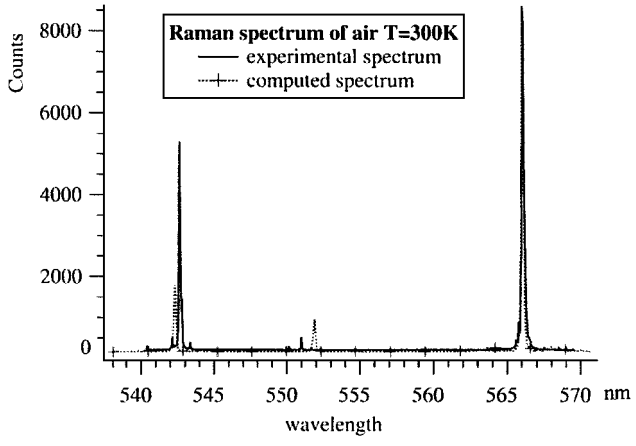

Fig. 13 Experimental Raman Stokes spectrum of air: $T_v = T_r = 300$ K.

static-pressure records (not represented here), the starting phase of the nozzle lasts about 600 μs from the opening of the secondary diaphragm. Likewise, from the pitot-pressure records (Fig. 9) and time-resolved emission records (Fig. 12) the steady phase ends at 1100 μs. Thus, this steady phase lasts about 500 μs at least for the free flow at the nozzle exit. However, pressure fluctuations, important during the first 300 μs of this phase (Figs. 9 and 12), point out that the part really stationary around the model only last 200 μs between 900 and 1100 μs. Raman measurements are operated during this period. Conditions 3 are much less drastic (Fig. 9).

Raman-Scattering Diagnostic and Data Reduction

As analyzed above, runs are performed with the laser pulse triggered during the steady phase, in which the expanding gas coming from the nozzle has constant aerodynamic and spectroscopic properties.

Raman-Scattering Diagnostic and Experimental Setup

SRS is a nonintrusive linear optical diagnostic very attractive for direct measurements of the vibrational population because it allows the recording of several Raman spectra in a spectral bandwidth of a few tens of nanometers with no overlapping nor quenching effects. The Raman shift is characteristic of the scattering molecule, and the intensity is linearly dependent of its concentration.

In Fig. 13 an experimental Raman Stokes spectrum of an N_2/O_2 mixture at a pressure of 0.1 Mpa and temperatures $T = T_r = T_v$ equal to 300 K is represented: this spectrum corresponds to a static measurement (without flow) in the test section of the tunnel.

Fully described theory and practical applications can be found in various books.[17,18] So, for an incident laser wavelength at 500.0 nm the nitrogen Stokes Q branch head corresponding to the vibrational transition $v = 1$ to 0 is at 565.9 nm; the Stokes Q branch head corresponding to the transition $v = 2$ to 1 is 0.93 nm downwards from the preceding one; the $v = 3$ to 2 transition is also 0.93 nm closer to the laser wavelength and so on.

The spectra obtained in conditions 1 and 3 with examples given in Figs. 5 and 6 effectively include Raman lines, and their analysis may therefore be operated. However, many difficulties remain as for their interpretation. The most important comes from the fact that, in the wavelength range including these lines, a few emission lines are still present and even some may overlap the Raman lines. The first rule therefore is to eliminate each line nonstrictly corresponding to the theoretical wavelengths for the transitions just defined and with an uncertainty of ± 0.1 nm. If there is overlapping with emission lines, the Raman line will be analyzed from the location of its maximum, if any, and assuming a theoretical shape consistent with the local conditions.

Data Reduction

Thus, each vibrational band is localized and identified as being a Raman Stokes Q branch part, and a computer peak fitting is performed to fit the well-reproducible baseline (caused by the thermal and readout noises) and the vibrational peaks. Because the intensity of the $v + 1$ to the v Raman Stokes transition scales as $v + 1$ times the vibrational population N_v, the summation of all rotational level transition intensities of the vibrational level of interest is equal to the area of this peak divided by $v + 1$. This operation, strictly valid for a harmonic oscillator, brings negligible error when applied to the first four levels of nitrogen. After performing these operations for all identified vibrational peaks, the deduced populations are normalized by the population of the $v = 0$ level N_0. Like other scattering phenomena, Raman scattering has a standard deviation on the intensities given by a Poisson distribution: $\sigma = (N_p)^{1/2}$. Photon counting experiments gives 50 counts per photon, and so the intensity errors are calculated to be $\pm 14\%$. Another source of error may be the calculation of the area assumed to be the sum of rotational transitions in a selected vibrational level. But the effects of vibrational temperature T_v and rotational (or, in our case, translational) temperature T_r are quite different on the Raman spectra. Increasing T_v leads to an increased population on the upper vibrational levels, and so the ratio of intensities of vibrational levels changes; thus, the peak heights change approximately in a similar way. When T_r increases, the ratio of intensities of vibrational levels remain the same, but the peak widths are extended. When T_r reaches a given value, the tail of the rotational structure of a level overlaps the adjacent upper level. The estimation of the area of vibrational transition intensities becomes much more difficult. Figure 14 represents calculated Raman Stokes spectra for nitrogen, assuming vibrational and rotational Boltzmann distributions. The maximum intensities are arbitrarily reduced to one in order to show the effects of T_v and T_r on the spectra; fortunately, because of the low value of T_r this point is not critical in the case of the experiments hereafter exposed.

However, when there is overlapping with parasitic lines the error already estimated of 14% must be largely doubled, so that the total

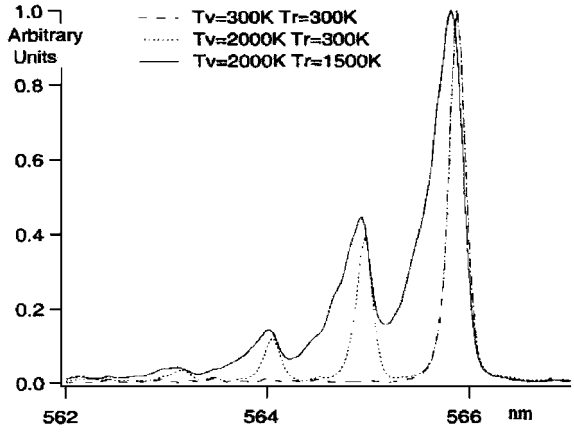

Fig. 14 Effects of T_v and T_r on Raman Stokes spectra of nitrogen.

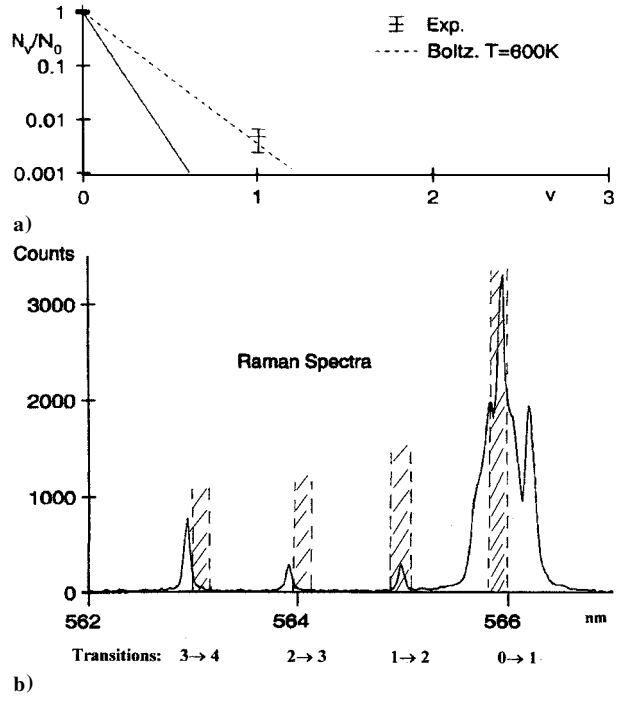

Fig. 15 Experimental Raman Stokes nitrogen spectrum at 4 mm in front of the model, conditions 3: a) relative populations and b) spectrum. ¦¦, possible location domains of Raman lines.

error, including also the uncertainties on the line location (±0.1 nm), can be estimated to about 40–50%.

SRS Measurements: Conditions 3

For conditions 3, corresponding to low temperatures, only SRS spectra coming from the flow behind the bow shock in front of the model are available because it is practically impossible to detect Stokes, and, a fortiori, anti-Stokes bands coming from levels different from the first one (level zero) in the free flow, the temperatures being too low, as previously noted. Thus, in the shock layer an example of the recorded spectrum obtained at 4 mm from the stagnation point is represented in Fig. 15: this spectrum corresponds to the wavelength range in which Stokes lines may appear (Fig. 15b). In the same plot theoretical positions of the lines corresponding to transitions from the vibrational levels 0, 1, 2, and 3 are also represented with an uncertainty of ±0.1 nm. Before giving any interpretation about populations, the preceding considerations indicate that the lines close to the Stokes lines $2 \rightarrow 3$ and $3 \rightarrow 4$ are practically outside the possible locations of these Stokes lines and therefore cannot be taken into account: they probably are emission lines including, or not, the Stokes lines. On the contrary, the $1 \rightarrow 2$ transition (565.0 nm) is clearly distinguishable as well as the $0 \rightarrow 1$ at 565.9 nm. This last line, however, is overlapped by other parasitic lines, but can be easily identified and interpreted owing to its visible maximum.

Then, computation of the relative populations of levels 1 and 0, N_1/N_0, can be operated by the just described method: the resulting relative population is plotted in Fig. 15a and compared with a Boltzmann distribution corresponding to the stagnation temperature 600 K. The agreement is satisfactory, which is not surprising, because the computed values of the temperatures T and T_v ahead of the detached shock are respectively 70 and 560 K. In the recompressed flow behind this shock, close to the stagnation point these temperatures are both close to 600 K.

This result can be considered as a good agreement between the computation and the experiment. If the lines close to 564 and 563 nm were considered respectively as the Stokes lines $2 \rightarrow 3$ and $3 \rightarrow 4$, the computation of the corresponding populations would give a very strong overpopulation of the corresponding levels 2 and 3 (not represented).

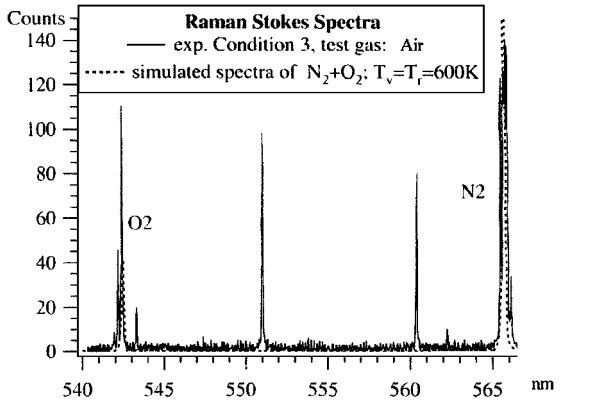

Fig. 16 Experimental Raman Stokes air spectrum at 4 mm in front of the model: conditions 3.

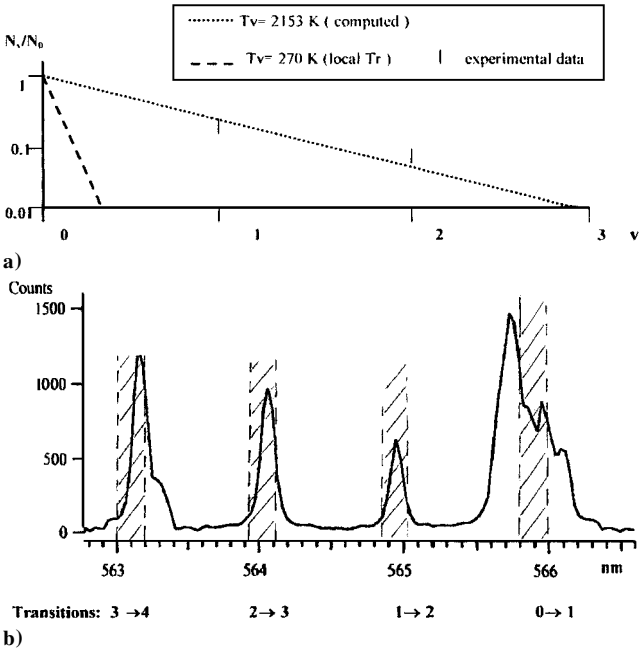

Fig. 17 Experimental Raman Stokes nitrogen spectrum in the freestream, conditions 1: a) relative populations and b) spectrum. ¦¦, possible location domains of Raman lines.

The same initial conditions are used with reconstituted air as a test gas, and the experimental spectrum is reported in Fig. 16. The parameters M_s and P_0 are identical, but only the $0 \rightarrow 1$ transition is visible for N_2. The same transition is also visible for O_2 in the same spectrum. Moreover, the line at 551 nm might be caused by Raman Stokes branch of NO, which could be a proof of the (surprising) presence of this gas at this low temperature: this has been found in another facility.[15] Because of some misalignment, the intensities of the Raman bands are very weak and correspond only to a few photons, and so no quantitative analysis has been made.

SRS Measurements: Conditions 1

For conditions 1 an example of the spectrum obtained in the freestream at the nozzle exit is presented in Fig. 17b. As with the conditions 3, it is clear that the Stokes line corresponding to the transition $0 \rightarrow 1$ is overlapped by emission lines, but, in the present case, the identification is more unreliable. However, the secondary maximum of this spectrum part is included in the possible location domain of the Stokes line $0 \rightarrow 1$ and thus can be considered as the center of this line. On the other hand, the Stokes lines $1 \rightarrow 2$ and $2 \rightarrow 3$ are clearly identifiable. This is however not the case for the $3 \rightarrow 4$ line, apparently concealed by a strong emission line.

Thus, the first three Stokes lines are taken into account, and the relative populations of levels 0, 1, 2 are computed. The results are

reported in Fig. 17a, and compared to the Boltzmann distribution at $T_v = 2153$ K and $T = 270$ K temperatures given by the just cited Navier–Stokes computation.[15] The agreement is also quite satisfactory and can be considered as a validation of the physical and computational models.

It is also remarkable that, if the line close to the $3 \rightarrow 4$ Raman line was taken into account, the population of the level 3 would be much larger than the expected Boltzmann population. This is either unrealistic or would come from the presence of impurities, as it has been found in old experiments[6] or, more recently, in an arc tunnel,[19] but it does not seem the case in shock tubes.[20]

Conclusions

New reliable and stable running conditions have been defined in the hypersonic facility TCM2 increasing its potentialities toward low temperatures and high pressures. The possibility of determining the useful test time accurately also represents an additional step in the control of experiments. Concurrently, the development, difficult but feasible, of a spontaneous Raman scattering technique gives the possibility of obtaining vibrational populations in a nonequilibrium hypersonic flow. Thus, the population of the first vibrational levels corresponds to a Boltzmann distribution defined at temperatures, translational and vibrational, given by classical Landau–Teller computations, as already shown by other recent experiments,[12] operated however in much weaker expansion conditions. This also means that the relaxation process does not differ in compression or expansion (strong and weak) conditions and that simple and global models are sufficient for the determination of the macroscopic parameters of hypersonic expanded flows. However, the possibility of overpopulation of higher levels, perhaps caused by the presence of impurities exciting the corresponding nitrogen molecules, cannot be excluded in the large facilities. This conclusion, however, remains uncertain because of the overlapping of Raman lines by residual emission lines, themselves caused by radiation of impurities. Thus, efforts must be made to obtain a clean setup, although their effect must not be overestimated.[20] Moreover, measurements of the same type should be operated in the reservoir itself, and other Raman spectroscopy experiments, spontaneous or coherent, should be to plan in higher stagnation enthalpy conditions including significant chemical reactions.

Acknowledgments

We gratefully acknowledge the support of European Space Agency, especially J. Muylaert, and of Centre d'Etudes Scientifiques et Techniques d'Aquitaine, especially G. Duffa and J. Cousi.

References

[1]McIntyre, T. J., Bishop, A. I., Thomas, A. M., Wegener, M. J., and Rubinstein-Dunlop, H., "Emission and Holographic Interferometry Measurements in a Superorbital Expansion Tube," *AIAA Journal*, Vol. 36, No. 6, 1998, pp. 1049–1054.

[2]Beck, W. H., Trinks, O., and Mohammed, A., "Characterisation of High Enthalpy Flows Using Diode Laser Absorption Spectroscopy of Nitric Oxide and Rubidium," *Proceedings of the 22nd International Symposium on Shock Waves*, edited by G. J. Ball, R. Hillier, and G. T. Roberts, Vol. 1, Imperial College, London, 1999, pp. 347–352.

[3]Chaix, A., Dumitrescu, M. P., Dumitrescu, L. Z., and Brun, R., "Calibration of the TCM2 Conical Nozzle and Internal Flow Investigation," *Proceedings of the 21st International Symposium on Shock Waves*, edited by A. F. P. Honwing, Great Keppel, Queensland, Australia, 1997, pp. 1–6.

[4]Brun, R., Burtschell, Y., Chaix, A., Druguet, M. C., Dumitrescu, L. Z., Dumitrescu, M. P., Martin, R., and Zeitoun, D., "Flow in the TCM2 Marseille Hypersonic Facility: Some New Experimental Results," *Proceedings of the 20th International Symposium on Shock Waves*, edited by B. Sturtevant, J. E. Shepherd, and H. G. Hornung, Vol. 1, World Scientific, Singapore, 1995, pp. 227–232.

[5]Stalker, R. J., "Recent Development with Free Piston Drivers," *Proceedings of the 17th International Symposium on Shock Waves*, edited by Y. W. Kim, American Institute of Physics, New York, 1990, pp. 96–105.

[6]Hurle, I. R., Russo, A. L., and Hall, J. G., "Spectroscopic Studies of Vibrational Nonequilibrium in Supersonic Nozzle Flows," *Journal of Chemical Physics*, Vol. 40, No. 8, 1964, pp. 2076–2089.

[7]Millikan, R. C., and White, D. R., "Systematics of Vibrational Relaxation," *Journal of Chemical Physics*, Vol. 39, No. 12, 1963, pp. 3209–3213.

[8]Caledonia, G. E., and Center, R. E., "Vibrational Distribution Functions in Anharmonic Oscillators," *Journal of Chemical Physics*, Vol. 39, No. 12, 1971, pp. 3209–3213.

[9]Von Rosenberg, C. W., Taylor, R. L., and Teare, J. D., "Vibrational Relaxation of CO in Nonequilibrium Nozzle Flow and the Effect of Hydrogen Atoms on CO Relaxation," *Journal of Chemical Physics*, Vol. 54, No. 5, 1971, pp. 1974–1987.

[10]Sebacher, D. I., and Guy, R. W., "Vibrational Relaxation in Expanding Nitrogen and Air," NASA TMX 71988, No. 74-31762, Aug. 1974.

[11]Teare, J. D., Taylor, R. L., and Von Rosenberg, C. W., "Observation of Vibration-Vibration Energy Pumping Between Diatomic Molecules," *Nature*, Vol. 225, Jan. 1970, pp. 240–243.

[12]Sharma, S. P., Ruffin, S. M., Gillespie, W. D., and Meyer, S. A., "Vibrational Relaxation Measurements in an Expanding Flow Using Raman Scattering," *Journal of Thermophysics and Heat Transfer*, Vol. 7, No. 4, 1993, pp. 697–703.

[13]Park, C., "A Review of Reaction Rates in High Temperature Air," AIAA Paper 89-1740, June 1989.

[14]Shatalov, O. P., "Recommended Data on Rate Constants of Physical and Chemical Processes in N-O Atoms System," Inst. of Mechanics, Avogadro Center, Moscow State Univ., Moscow, Russia, May 1989.

[15]William, J., "Physico-Chemical Processes in High Enthalpy Expanded Flows: Application to the Arcjet Facility F4," Ph.D. Dissertation, Mécanique-Energétique, Univ. of Provence, Marseille, France, Dec. 1999.

[16]Brun, R., "Nonequilibrium Effects in High Speed Flows: Modeling and Experimentation," *Hypersonics, Vol. 1: Defining the Hypersonic Environment*, edited by J. J. Bertin, R. Glowinski, and J. Periaux, Birkhäuser, Boston, 1989, pp. 429–460.

[17]Long, D. A., *Raman Spectroscopy*, McGraw–Hill, New York, 1977, Chaps. 2, 3.

[18]Lapp, M., Goldman, L. M., and Penney, C. M., "Raman Scattering from Flames," *Science*, Vol. 175, No. 4, 1972, pp. 1112–1115.

[19]Blackwell, H. E., and Scott, C. D., "Measured Rotational and Vibrational Temperature Differences in Arcjet Shock Layers," AIAA Paper 92-3030, June 1992.

[20]Ramjaun, D., Dumitrescu, M. P., and Brun, R., "Kinetics of Free Radicals Behind Strong Shock Waves," *Journal of Thermophysics and Heat Transfer*, Vol. 13, No. 2, 1999, pp. 219–225.